

Article

Research of Surrounding Rock Control of Gob-Side Entry Retaining Based on Deviatoric Stress Distribution Characteristics

Zhiqiang Wang ^{1,2,3,4}, Jiao Zhang ^{1,*}, Jingkai Li ¹, Peng Wang ¹, Chao Wu ¹ and Lei Shi ¹

¹ School of Energy and Mining Engineering, China University of Mining and Technology (Beijing), Beijing 100083, China; wzhiqianglhm_new@126.com (Z.W.); jingkai0801@163.com (J.L.); wangpengshg@163.com (P.W.); wuchaokd@163.com (C.W.); cumtshilei@163.com (L.S.)

² State Key Laboratory of Coal Resources in Western China, Xi'an University of Science and Technology, Xi'an 710054, China

³ Beijing Key Laboratory for Precise Mining of Intergrown Energy and Resources, China University of Mining and Technology (Beijing), Beijing 100083, China

⁴ National Demonstration Center for Experimental Safe Coal Mining and Geological Guarantee Education, China University of Mining and Technology (Beijing), Beijing 100083, China

* Correspondence: zj33703370@163.com

Abstract: In view of the difficulty of the surrounding rock control of retaining a roadway along a goaf, this paper takes the 5504 working face of the Hongshuliang Coal Mine as the engineering context. The uniaxial compressive strength and tensile strength of concrete filling material in the retained roadway are determined by laboratory tests. Through theoretical analysis, field investigation, numerical simulation and field measurement, the distribution characteristics of deviatoric stress and damage zone of the roadway surrounding rock in the mining process of the 5504 working face are studied here. Based on the failure of rock mass element caused by deviatoric stress tensors, the study shows that the thickness of the concrete wall is 2.2 m and the compressive strength of the concrete wall can reach 10.87~11.64 MPa in 3 days to 4 days, which can meet the support strength of the retained roadway. From the position of 90 m in front of the working face to the position of 100 m behind the working face, the distribution form of the roadway surrounding rock deviatoric stress is: symmetrical butterfly shape → single butterfly shape → narrow oblique strip → oblique 8 shape → wide oblique strip shape. When the distance between the retained roadway and the working face is 49 m, the retained roadway tends to be stable. Based on the distribution characteristics of the deviatoric stress outline line and the damage zone outline line of the retained roadway surrounding rock, the retained roadway surrounding rock is divided into three regions, and the combined support technology of “bolt + anchor cable + single pillar + reinforcement combined with steel plate to strengthen concrete wall” is proposed. Through field engineering practice, the maximum displacement of roof, floor, solid coal side and concrete wall side in the retained roadway is 136.6 mm, 78.8 mm, 62.3 mm and 43.3 mm, respectively, and the surrounding rock control effect of the retained roadway is good.

Keywords: concrete wall; deviatoric stress; damage zone; surrounding rock control; gob-side entry retaining



Citation: Wang, Z.; Zhang, J.; Li, J.; Wang, P.; Wu, C.; Shi, L. Research of Surrounding Rock Control of Gob-Side Entry Retaining Based on Deviatoric Stress Distribution Characteristics. *Sustainability* **2022**, *14*, 5660. <https://doi.org/10.3390/su14095660>

Academic Editor:
Constantin Chaliotis

Received: 6 March 2022

Accepted: 4 May 2022

Published: 7 May 2022

Publisher's Note: MDPI stays neutral with regard to jurisdictional claims in published maps and institutional affiliations.



Copyright: © 2022 by the authors. Licensee MDPI, Basel, Switzerland. This article is an open access article distributed under the terms and conditions of the Creative Commons Attribution (CC BY) license (<https://creativecommons.org/licenses/by/4.0/>).

1. Introduction

No-pillar mining can raise the coal mining rate, prolong the life of the mine, reduce the amount of roadway excavation, control the gas overrun, etc. It is an advanced coal mining technology that is beneficial to improving the technical and economic effect of safety and production [1,2]. Therefore, gob-side entry retaining is widely used as a mining technology without a coal pillar. According to plastic mechanics, the plastic deformation of rock is mainly caused by deviatoric stress, which can control the distortion and failure of rock [3–6]. In recent years, many beneficial results have been achieved in the study of gob-side entry

and deviatoric stress. In terms of gob-side entry retaining technology, Tan [7–9] analyzed the characteristics of mine pressure under the condition of gob-side entry with hard roof and soft bottom and proposed the comprehensive control technology of surrounding rock. Du [10] studied the mechanical properties of filling materials in roadway and proposed a gob-side entry retaining technology without a coal pillar suitable for thin coal seam mining. Tian [11] analyzed the mechanical model of interaction between filling body and roof of soft roof, floor and gob-side entry retaining in thin coal seams and obtained the influencing factors of surrounding rock stability of soft roof, soft floor and gob-side entry retaining in thin coal seams. Luan [12] compared and analyzed the mechanical properties of lightweight high strength foam concrete and mortise-tenon hollow block wall, and optimized the labor efficiency of gob-side entry retaining technology. Zhang [13] studied the roof transfer and bearing mechanism of gob side in gob-side entry retaining and put forward the trinity control technology composed of high strength bolt, roof control support and roadside filling body. By analyzing the surrounding rock migration law of gob-side entry retaining in fully mechanized caving, Xie [14] systematically summarized the influence of main roof fracture position and filling body width on surrounding rock stability of gob-side entry retaining. Yu [15] used numerical simulation to analyze the instability of roadway surrounding rock under different stress conditions and proposed that roadway instability under different lateral pressure coefficients can be divided into typical normal symmetric instability mode and typical angular symmetric instability mode. In terms of deviatoric stress, Wang [16] studied the distribution law of deviatoric stress for surrounding rocks in gob-side entry. Ma [17] deduces the analytical expression of the deviatoric stress field of roadway surrounding rock and analyzes the plastic zone and deviatoric stress evolution law of roadway surrounding rock under different lateral pressure coefficient. Xu [18] simulated the distribution characteristics of the deviatoric stress field on the floor of the residual coal pillar of the coal seam; in the same horizontal plane, the deviatoric stress showed a saddle distribution, and with the increase of the width of the coal pillar, the deviatoric stress at the middle line and the edge of the coal pillar increased firstly and decreased continuously. Li [19] monitored the stress area of the roadway filling body and analyzed the failure mode of the filling body. The study shows that reducing the settlement space of the roof strata can prevent the filling body from producing excessive principal deviatoric stress.

The above achievements have enriched the research results of gob-side entry retaining, which has far-reaching guiding significance for the stability control of roadway surrounding rock. But when filling concrete wall is used to preserve roadways, there are few studies on the distribution law of deviatoric stress in the surrounding rock, especially the relationship between the final setting time of concrete wall and the distribution of deviatoric stress in surrounding rock of roadway. Therefore, taking the 5504 working face of Hongshuliang Coal Mine as the engineering context, the concrete curing time and mechanical properties of concrete filling material have been tested in the laboratory. The distribution characteristics of deviatoric stress and damage area of roadway surrounding rock are systematically studied. The roadway surrounding rock is divided into three regions with the boundary of the peak deviatoric stress outline line and the damage area outline line, and different supporting forms are used to control the roadway surrounding rock in the three regions. Through engineering practice, the subregional control technology of the roadway surrounding rock meets the needs of safe production in the mine. This technology can provide a reference for roadway support under similar conditions.

2. Engineering Context

The 5504 working face of the Hongshuliang Coal Mine is located in the No. 5 coal seam with a buried depth of 125~145 m and an average buried depth of 134.5 m. The average

thickness of the No. 5 coal seam is 3 m and the length of the 5504 working face is 170 m. The advancing speed of the 5504 working face is 2 m/d. The transportation roadway of the 5504 working face is driven along the roof and floor of the seam, and the width and height of the transportation roadway are 4 m and 3 m, respectively. The concrete wall is filled between the 5504 transportation roadway and the goaf. The 5504 transportation roadway is retained in situ as the material roadway of the 5505 working face. The comprehensive histogram of coal and rock strata is shown in Figure 1a, and the schematic diagram of the working face is shown in Figure 1b.

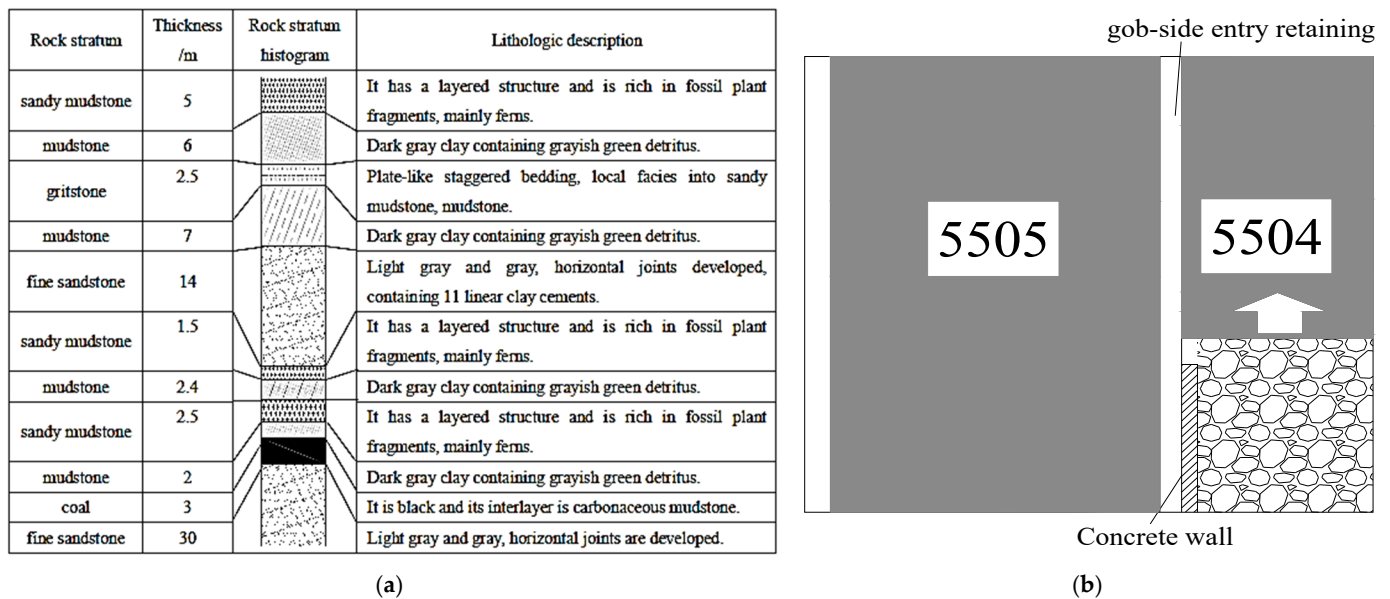


Figure 1. Three-dimensional schematic diagram of the working face. (a) Comprehensive histogram of coal strata; (b) The schematic diagram of the working face.

3. Strength Analysis of Concrete Materials

3.1. Analysis of Retained Roadway Support Strength

The calculation method of roadside support in gob-side entry generally adopts a superposition continuous plate model. In the superposition continuous plate model, each plate is allowed to be separated and dislocated, each plate can be regarded as an independent continuous plate structure and the plates are connected by a distributed load which is closer to reality [20]. To facilitate the solution, the superimposed plate loads are first divided and a strip with the largest load in each plate is selected as the calculation unit. In the selected strip area, the size and action position of the supporting force for gob-side entry are marked and the mechanical model of supporting–surrounding rock interaction is established.

As shown in Figure 2a, it is assumed that the uniformly distributed load of the roof is q and the load on the strip area is only distributed on the AB and CD sections. p represents the concentrated load of the filling body [21,22].

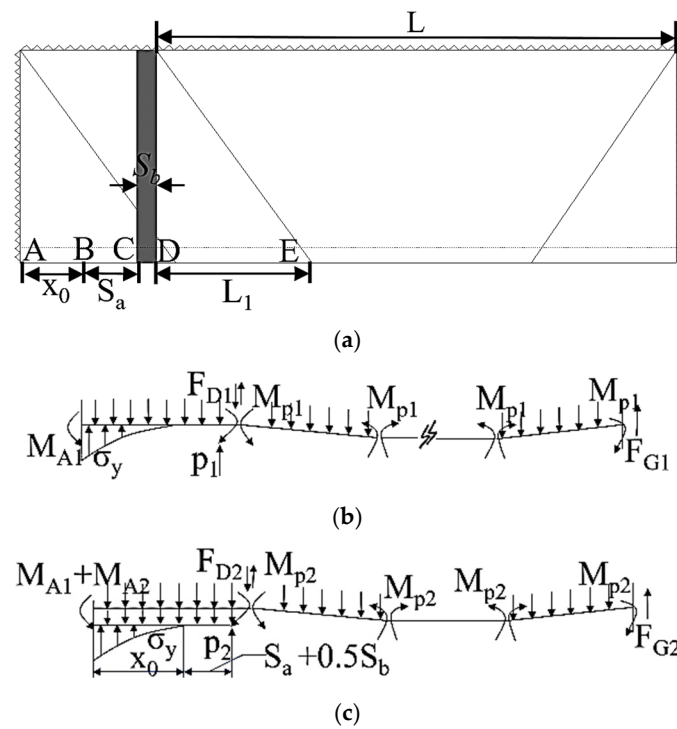


Figure 2. Calculation model of the support resistance for gob-side entry. (a) Regional diagram of roadway roof; (b) Direct roof of the first layer in the upper part of the coal seam; (c) The direct roof of the second layer in the upper part of the coal seam.

The rock layer below the key layer actively collapses. The equilibrium method is used to solve each section in the figure. The bending moment caused by stress in the rock layer is ignored and only the weight of the rock layer is considered. Because the coal around the roadway is affected by mining, the coal may loosen or even damage under the action of supporting pressure. Therefore, the coal wall around the roadway is not suitable as the supporting point of the roof of gob-side entry, and the junction between the loose area and plastic area of coal should be regarded as the fixed fulcrum or simple fulcrum of the roof of gob-side entry. In Figure 2b, σ_y and x_0 are the supporting stress and width of the stress limit equilibrium zone, respectively, which are calculated by the following Formulas (1) and (2).

$$\sigma_y = \left(\frac{C_0}{\tan \varphi} + \frac{P_x}{A} \right) \exp \frac{2 \tan \varphi}{MA} x - \frac{C_0}{\tan \varphi} \tag{1}$$

$$x_0 = \frac{MA}{2 \tan \varphi} \ln \frac{K\gamma H + \frac{C_0}{\tan \varphi}}{\frac{C_0}{\tan \varphi} + \frac{P_x}{A}} \tag{2}$$

where C_0 , φ , P_x , A , γ , K and H represent the cohesive force at the interface between coal seam and roof and floor strata, the internal friction angle at the interface between coal seam and roof and floor strata, the supporting strength of coal side, the coefficient of lateral pressure, the average volume-weight of the overlying strata, the coefficient of stress concentration and the buried depth of the coal seam, respectively.

The stress analysis of the first layer on the upper part of coal seam is shown in Figure 2b.

In the DE segment:

$$\sum F_y = 0 \quad F_{D1} = q_1 L_1 \tag{3}$$

$$\sum M = 0 \quad M_{p1} = \frac{q_1 L_1^2}{4} \tag{4}$$

In the *AD* segment:

$$\begin{aligned} \Sigma M = 0 \\ M_{A1} - M_{P1} - \frac{1}{2}q_1(S_a + S_b + x_0)^2 - F_{D1}(S_a + S_b + x_0) + P_1\left(S_a + \frac{S_b}{2} + x_0\right) + \int_0^{x_0} \sigma_y(x_0 - x)dx = 0 \end{aligned} \quad (5)$$

Under the limit condition, $M_{A1} = M_{P1}$. The simultaneous Formulas (3)–(5) are obtained:

$$P_1\left(S_a + \frac{S_b}{2} + x_0\right) = \frac{1}{2}\gamma_1 h_1(S_a + S_b + x_0)^2 + \gamma_1 h_1(S_a + S_b + x_0)L_1 - \int_0^{x_0} \sigma_y(x_0 - x)dx \quad (6)$$

where M_{P1} , M_{A1} , F_{D1} , P_1 , q_1 , h , S_a , x_0 , L_1 and S_b , respectively, represent the ultimate bending moment of rock stratum, the bending moment of rock stratum, the shear force at point *D*, the resistance to cutting the roof, gravity concentration of rock stratum, the thickness of rock stratum, the width of roadway, the width of the loose area of coal, the characteristic dimension of rock stratum breaking and width of filling body.

Stress analysis of the second layer of the direct roof at the upper part of the coal seam is shown in Figure 2c.

In the *DE* segment, similarly, due to $\Sigma F_y = 0$ and $\Sigma M = 0$, obtain:

$$\begin{aligned} M_{A1} + M_{A2} + P_2\left(S_a + \frac{S_b}{2} + x_0\right) - M_{P2} - \frac{1}{2}\gamma_2 h_2(S_a + S_b + x_0 + h_{z1} \tan \alpha)^2 - \frac{1}{2}\gamma_1 h_1(S_a + S_b + x_0)^2 - \\ F_{D2}(S_a + S_b + x_0 + h_1 \tan \alpha) - F_{D1}(S_a + S_b + x_0) + \int_0^{x_0} \sigma_y(x_0 - x)dx = 0 \end{aligned} \quad (7)$$

where F_{D1} , F_{D2} and α are the shear forces at the *D* point after the fracture of the first, second strata, respectively, and rock breaking angle.

Formula (7) can be rewritten as:

$$\begin{aligned} P_2\left(S_a + \frac{S_b}{2} + x_0\right) = \frac{1}{2}\sum_{i=1}^2 \gamma_i h_i \left(S_a + S_b + x_0 + \sum_{j=0}^{i-1} h_j \tan \alpha\right)^2 + \sum_{i=1}^2 F_{Di} \left(S_a + S_b + x_0 + \sum_{j=0}^{i-1} h_j \tan \alpha\right) + \\ M_{P2} - \int_0^{x_0} \sigma_y(x_0 - x)dx - \sum_i M_{Ai} \end{aligned} \quad (8)$$

If there is m_i stratum below the key strata, the formula for calculating the resistance is as follows:

$$\begin{aligned} P_{mi}\left(S_a + \frac{S_b}{2} + x_0\right) = \frac{1}{2}\sum_{i=1}^{mi} \gamma_i h_i \left(S_a + S_b + x_0 + \sum_{j=0}^{i-1} h_j \tan \alpha\right)^2 + \sum_{i=1}^{mi} F_{Di} \left(S_a + S_b + x_0 + \sum_{j=0}^{i-1} h_j \tan \alpha\right) + \\ M_{pmi} - \int_0^{x_0} \sigma_y(x_0 - x)dx - \sum_{i=1}^{mi} M_{Ai} \end{aligned} \quad (9)$$

Because F_{Di} is mainly affected by the boundary of caved rock. Usually, when the thickness of the overlying rock is less than 2~4 times of mining height, the caved rock loses contact with the boundary. Therefore, $F_{Di} = 0$, Formula (9) becomes:

$$P_{mi}\left(S_a + \frac{S_b}{2} + x_0\right) = \frac{1}{2}\sum_{i=1}^{mi} \gamma_i h_i \left(S_a + S_b + x_0 + \sum_{j=0}^{i-1} h_j \tan \alpha\right)^2 + M_{pmi} - \int_0^{x_0} \sigma_y(x_0 - x)dx - \sum_{i=1}^{mi} M_{Ai} \quad (10)$$

The key strata caves under the combined action of weight and external load of overlying strata, that is, the passive collapse of the strata. Its mechanical model is similar to Figure 2c. For the convenience of analysis, the dead weight of the *i* layer is set as $\gamma_i H_i$ and the external load is set as q_i . If m_{i+1} layer is the key layer and $m_{i+1} \sim m$ layers collapse simultaneously with the key layer, the lower limit of support resistance is:

$$\begin{aligned} P_m\left(S_a + \frac{S_b}{2} + x_0\right) = \frac{1}{2}\sum_{i=1}^m \gamma_i h_i \left(S_a + S_b + x_0 + \sum_{j=0}^{i-1} h_j \tan \alpha\right)^2 + M_{pm} - \sum_{i=1}^m M_{Ai} - \int_0^{x_0} \sigma_y(x_0 - x)dx + \\ \frac{1}{2}\sum_{i=m+1}^m \left[q_i \left(S_a + S_b + x_0 + \sum_{j=0}^{i-1} h_j \tan \alpha\right) \right]^2 + \sum_{i=m+1}^m \left[q_i \left(S_a + S_b + x_0 + \sum_{j=0}^{i-1} h_j \tan \alpha\right) L_i \right] \end{aligned} \quad (11)$$

In Formula (11) above, the roadway support in advance can significantly improve the bending ability of rock strata (ΣM_{Ai}) and reduce the support resistance of concrete walls.

To facilitate the calculation of the upper limit value of support resistance, assuming $\Sigma M_{Ai} = 0$, it is obtained from the Formula (11):

$$P_m \left(S_a + \frac{S_b}{2} + x_0 \right) = \frac{1}{2} \sum_{i=1}^{mi} \gamma_i h_i \left(S_a + S_b + x_0 + \sum_{j=0}^{i-1} h_j \tan \alpha \right)^2 + M_{pm} - \int_0^{x_0} \sigma_y (x_0 - x) dx + \frac{1}{2} \sum_{i=mi+1}^m \left[q_i \left(S_a + S_b + x_0 + \sum_{j=0}^{i-1} h_j \tan \alpha \right) \right]^2 + \sum_{i=mi+1}^m \left[q_i \left(S_a + S_b + x_0 + \sum_{j=0}^{i-1} h_j \tan \alpha \right) L_i \right] \quad (12)$$

3.2. Compressive Strength Test of Concrete Specimens

The 5504 working face is filled with concrete walls in the transportation roadway to retain the transportation roadway. The function of the concrete wall is to close the goaf, cut off the roof and reduce the separation of overlying strata [23]. The filling material of Hongshuliang Coal Mine is composed of cement, sand, rubble, water, concrete pumping agent (FDN-3), early strength water reducing agent (EHD) and sodium meta aluminate (P0102). The raw material and water–cement ratio is shown in Table 1.

Table 1. The raw material ratio and water–cement.

Raw Material	Cement	Sand	Rubble	Water	FDN-3	EHD	P0102
Mass (kg)	500	820	850	226	1.2	4	0.3
Proportion of mass (%)	20.82	34.14	35.39	9.41	0.05	0.2	0.01

According to the above material ratio, the standard cylinder specimens with the specification of $\phi 50 \text{ mm} \times 100 \text{ mm}$ and $\phi 50 \text{ mm} \times 25 \text{ mm}$ are manufactured. The uniaxial compressive strength, the elastic modulus, the Poisson's ratio and tensile strength of concrete specimens are tested. The relationship between the mechanical properties of concrete specimens and curing time is shown in Figure 3.

It can be seen from Figure 3 that with the increase of curing time, the uniaxial compressive strength, tensile strength and elastic modulus of concrete increase, and Poisson's ratio decreases. However, the daily change rate of uniaxial compressive strength, tensile strength, elastic modulus and Poisson's ratio is the curve shape of upper and lower fluctuations. The curing time of 1~3 days is the rapid growth period of the mechanical parameters of concrete. In the rapid growth period, the compressive strength of concrete increases from 2.55 MPa to 10.87 MPa, the tensile strength of concrete increases from 0.1 MPa to 0.9 MPa, the elastic modulus increases from 0.514 GPa to 2.148 GPa and Poisson's ratio decreases from 0.3 to 0.23. The curing time from 4 days to 24 days is the slow increasing period of mechanical parameters of concrete. In the slow increasing period, the compressive strength of concrete increases from 11.64 MPa to 27.83 MPa, the tensile strength of concrete increases from 0.92 MPa to 1.8 MPa, the elastic modulus increases from 2.248 GPa to 4.158 GPa and Poisson's ratio decreases from 0.2 to 0.152. When the curing time is 25 days or more, the compressive strength, tensile strength, elastic modulus and Poisson's ratio of the concrete are 28.21 MPa, 1.8 MPa, 4.154 GP and 0.152, respectively.

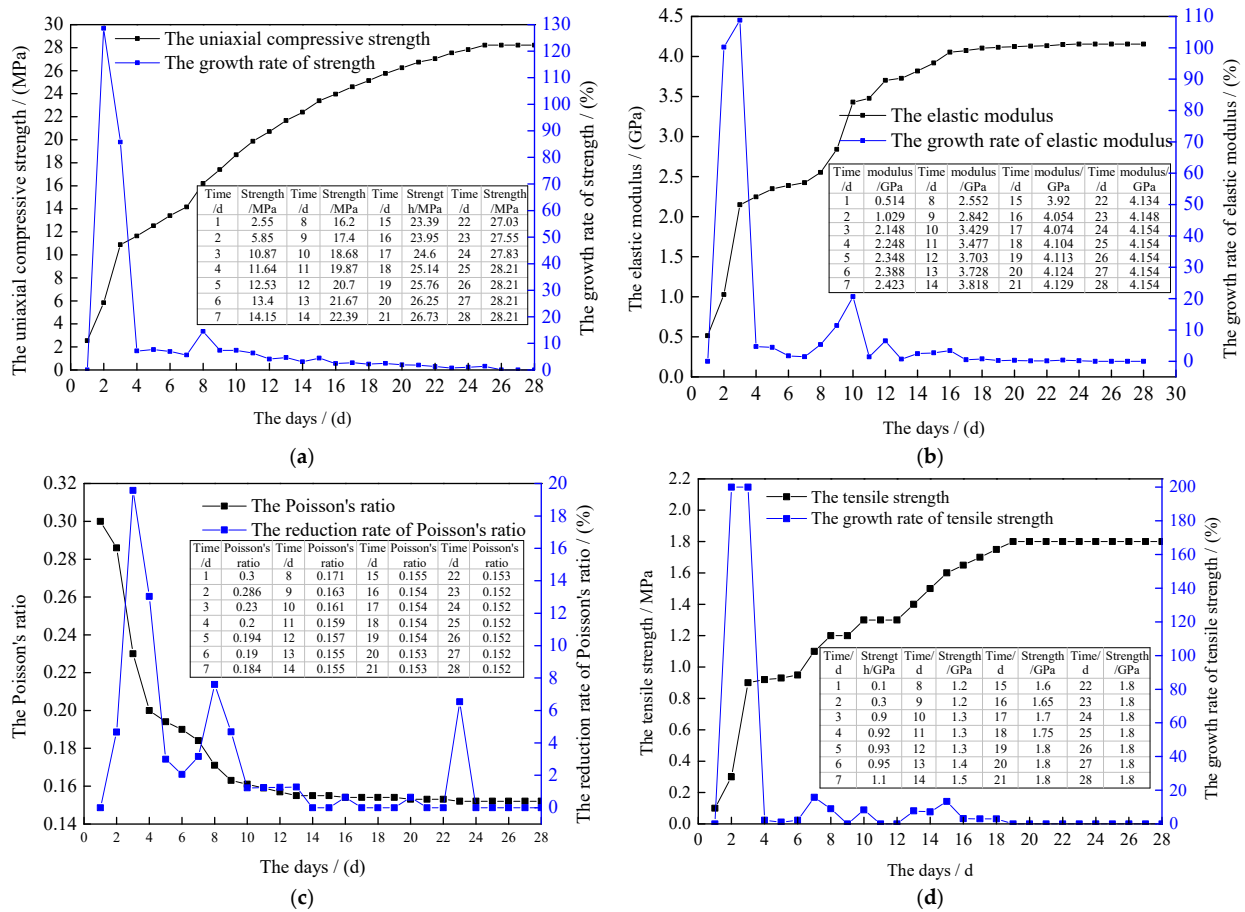


Figure 3. The relationship between the mechanical properties of concrete specimens and curing time. (a) The uniaxial compressive strength; (b) The elastic modulus; (c) The Poisson’s ratio; (d) The tensile strength.

3.3. Width and Support Strength of Concrete Wall

By substituting the mechanical parameters in Table 2 into Formulas (11) and (12), the relationship between roadway support strength, roadway width and concrete wall width changes, as shown in Figure 4.

Table 2. Mechanical parameters of roadway.

Symbol of the Parameter	$S_b/(m)$	$L_1/(m)$	A	P_x	K	$H/(m)$	$C_0/(MPa)$	$\varphi/(^\circ)$	$q_1/(KPa)$
Parameters	1.2~3	8.7	0.5	0	2	134.5	0.3	25	49
Symbol of the parameter	$S_a/(m)$	$q_2/(KPa)$	$q_3/(KPa)$	$q_4/(KPa)$	$q_5/(KPa)$	$q_6/(KPa)$	$q_7/(KPa)$	$q_8/(KPa)$	$q_9/(KPa)$
Parameters	3~5.5	63	58	37	818	242	117	164	126

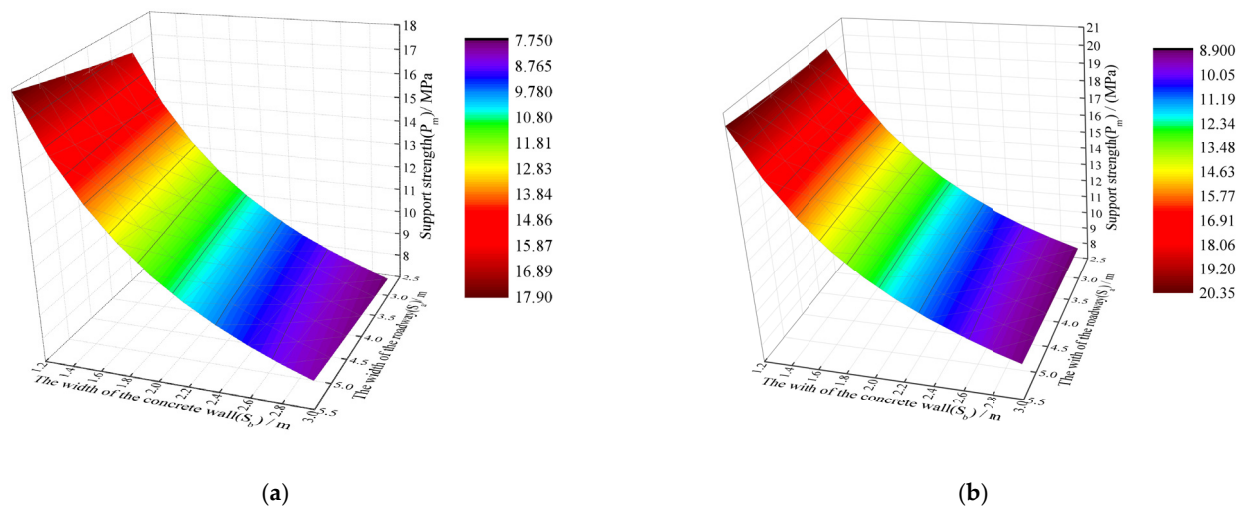


Figure 4. The relationship between roadway support strength, roadway width and concrete wall width. (a) Lower limit of support strength; (b) Upper limit of support strength.

As shown in Figure 4, when the width of gob-side entry is unchanged, the support strength decreases greatly with the increase of concrete wall width. Similarly, when the width of the concrete wall is constant, the support strength tends to increase slightly with the increase of the width of the gob-side entry retaining. Therefore, the supporting strength of the concrete wall is affected by both the width of the retained roadway and the width of the concrete wall, and the width of the concrete wall has a greater impact on the supporting strength.

According to the field measurement, the impel speed of nearby coal face is 2 m/d and the average distance of periodic pressure on the working face is about 8 m to 9 m. Comprehensively considering the relationship between Figures 3 and 4, the impel speed of working face and periodic pressure, when the width of retained roadway is 4 m and the width of concrete wall is 2.2, the required support strength of retained roadway is 10.16~11.64 MPa, while the compressive strength of concrete wall can reach 10.87~11.64 MPa after 3~4 days, so the reasonable width of concrete wall is 2.2 m.

4. Numerical Simulation

4.1. Simulation of Concrete Material

The version of FLAC3D is 5.01, developed by American Itasca Company, and the software is from Beijing, China. In order to obtain the parameters of the concrete material in FLAC3D software that, a cylinder model with the specification of 50 mm \times 100 mm was established in FLAC3D software. The parameters of elastic modulus, tensile strength and Poisson's ratio in Figure 3 were input into the model, and then different mechanical parameters, such as cohesion and internal friction angle, were substituted. The speed of 2×10^{-5} m/steps was applied at the top and bottom of the cylinder model, respectively. The stress–strain curve in FLAC3D software was compared with the stress–strain curve in the laboratory, and the variation curves of cohesion and internal friction angle of concrete were obtained, as shown in Figure 5.

As shown in Figure 5, when the curing time of concrete material is 1~3 days, the internal friction angle increases from 15 to 39.5° and the cohesion increases from 0.5 MPa to 1.1 MPa. When the curing time of concrete is 4~24 days, the internal friction angle increases from 40 to 45° and the cohesion increases from 1.2 MPa to 3.7 MPa.

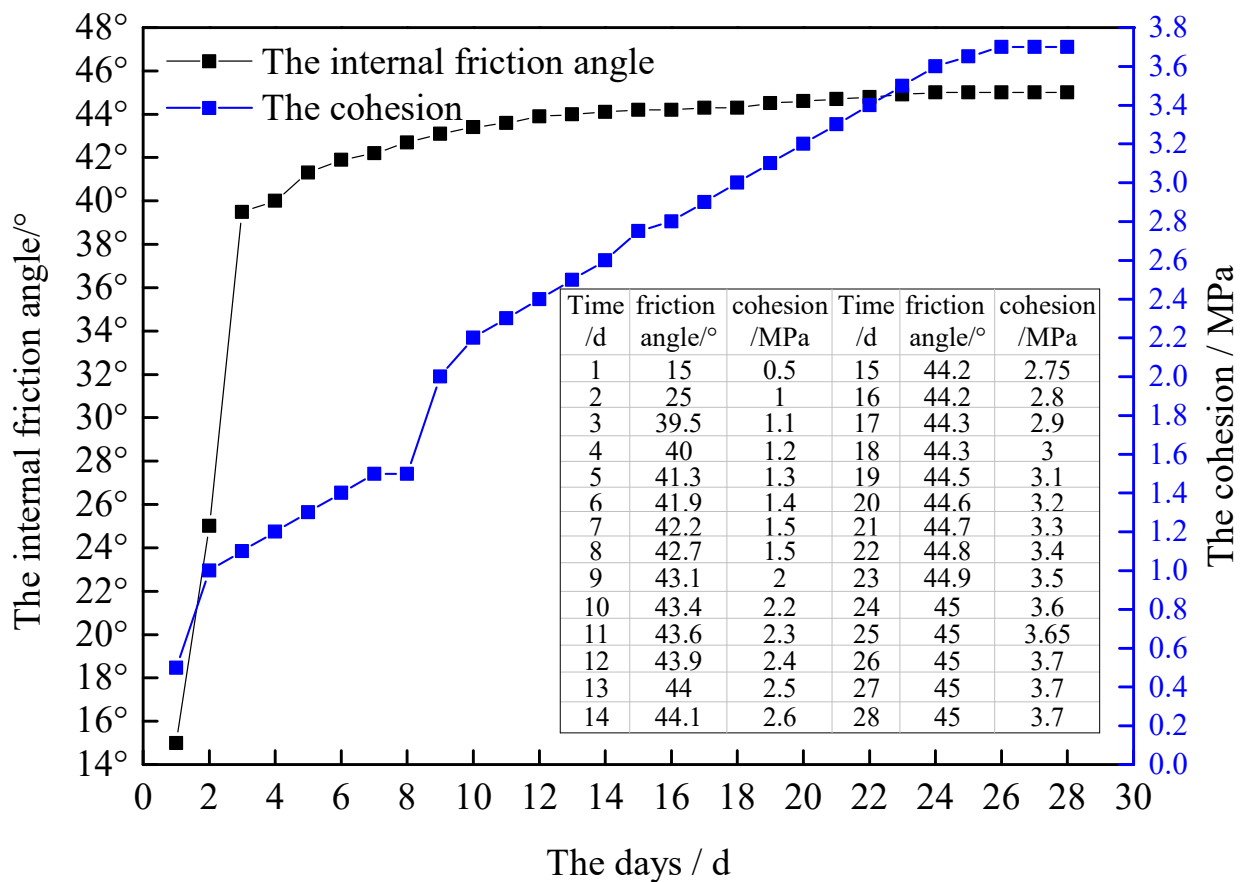


Figure 5. The relationship between the mechanical parameters of materials and curing time.

4.2. Overview of Indicators of Deviatoric Stress

In elastic–plastic mechanics, the stress tensor is divided into a spherical stress tensor and a deviatoric stress tensor. When the stress state at a point in the rock mass is represented by the principal stress (σ_i), it is divided into three principal stresses that are perpendicular to each other.

$$\begin{pmatrix} \sigma_1 & 0 & 0 \\ 0 & \sigma_2 & 0 \\ 0 & 0 & \sigma_3 \end{pmatrix} = \begin{pmatrix} \sigma_m & 0 & 0 \\ 0 & \sigma_m & 0 \\ 0 & 0 & \sigma_m \end{pmatrix} + \begin{pmatrix} \sigma_1 - \sigma_m & 0 & 0 \\ 0 & \sigma_2 - \sigma_m & 0 \\ 0 & 0 & \sigma_3 - \sigma_m \end{pmatrix} \quad (13)$$

$$\sigma_m = \frac{1}{3} \sum_1^3 \sigma_i \quad (14)$$

In Formula (13), the first term on the right is the spherical stress tensor (σ_m), which causes only volume changes of rock mass element. The second term on the right is the three deviatoric stress tensors that cause the fracture of the rock mass element, where $\sigma_1 - \sigma_m$ is the maximum deviatoric stress tensor. In this paper, the maximum deviatoric stress ($\sigma_1 - \sigma_m$) is applied to analyze the failure characteristics and evolution of the surrounding rock for gob-side entry.

4.3. Establishment of Working Face Model

The geological conditions of the 5504 working face are simple, without faults and initial large cracks. The size of the model is 250 m × 250 m × 95 m (length × width × height). The horizontal displacement of the boundary around the model is constrained, and the vertical displacement of the bottom boundary is constrained. The equivalent load of 3.07 MPa is applied to the upper part of the model to replace the overlying strata. The model adopts the

Coulomb–Mohr constitutive model. The mechanical parameters of the model are shown in Table 3 and the model is shown in Figure 6.

Table 3. Mechanical parameters of coal and rock mass.

Rock Strata	Density (kg/m ³)	Tensile Strength (MPa)	Cohesion (MPa)	Friction Angle (°)	Bulk Modulus (GPa)	Shear Modulus (GPa)
Overlying rock	2580	0.85	1.9	37	3.3	2.5
Sandy mudstone	2520	0.71	1.18	35	4.9	3.2
Mudstone	2437	0.53	0.7	30	4.3	2.8
Gritstone	2660	1.1	1.4	35	5.7	3.4
Mudstone	2437	0.53	0.7	30	4.3	2.8
Fine sandstone	2597	0.95	2.1	42	15.28	11.2
Sandy mudstone	2520	0.71	1.18	35	4.9	3.2
Mudstone	2437	0.53	0.7	30	4.3	2.8
Sandy mudstone	2520	0.71	1.18	35	4.9	3.2
Mudstone	2437	0.53	0.7	30	4.3	2.8
Coal	1460	0.3	0.3	25	1.3	0.63
Fine sandstone	2597	0.95	2.1	42	15.28	11.2
Concrete	2456	1.8	3.4	45	1.99	1.8

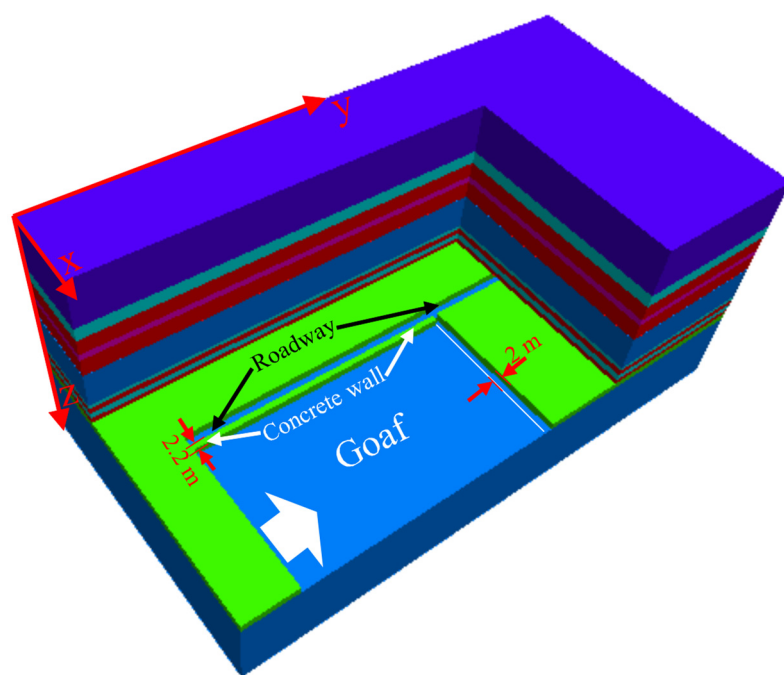


Figure 6. Numerical simulation model.

The process of the simulation is as follows:

1. At 40 m, 40 m and 50 m from the edge of the model, the haulage roadway, the auxiliary haulage roadway and the open-off cut of the working face are excavated to form the working face, as shown in Figure 7.
2. In the 5504 working face, the advancing distance of each mine is 2 m. The filling length of the concrete wall is 2 m each time. The distance between the end of the concrete wall and the 5504 working face is 2 m.
3. The concrete walls at different positions and at different times are given different strength values, that is, the strength of the concrete wall near the working face is lower and the strength of the concrete wall far away from the working face is higher. As in Figure 8, “*i*” represents the serial number of the concrete wall from the mining working face to the open-off cut of working face. When “*i* = 1” is the mechanical parameter of concrete curing for 1 day, “*i* = 2” is the mechanical parameter of concrete

curing for 2 days and “ $i = 3$ ” is the mechanical parameter of concrete curing for 3 days; until “ $i = 24$ ” or above, the mechanical parameter will not be re-assigned.

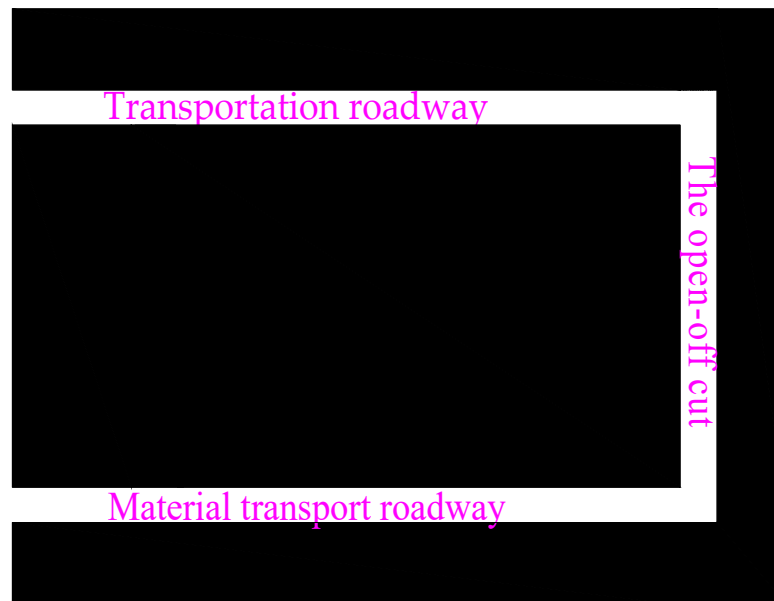


Figure 7. Schematic diagram of roadway layout.

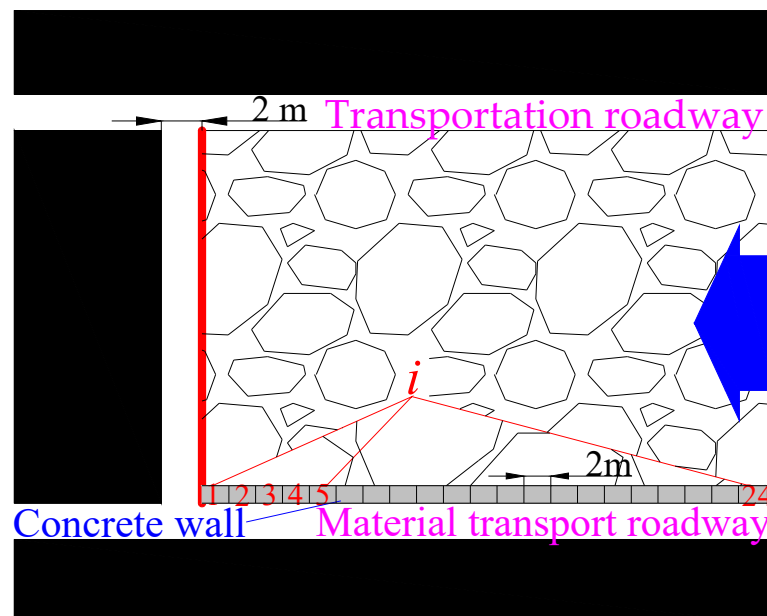


Figure 8. Layout of the filling wall.

4.4. Deviatoric Stress Distribution Law

4.4.1. Deviatoric Stress Distribution Law at Different Section Positions

In the axial direction of the reserved roadway, the position of the working face is 0 m. The range greater than 0 m is unmined and the range less than 0 m is the mined-out area. In different section positions of the roadway, the distribution of deviatoric stress is shown in Figure 9.

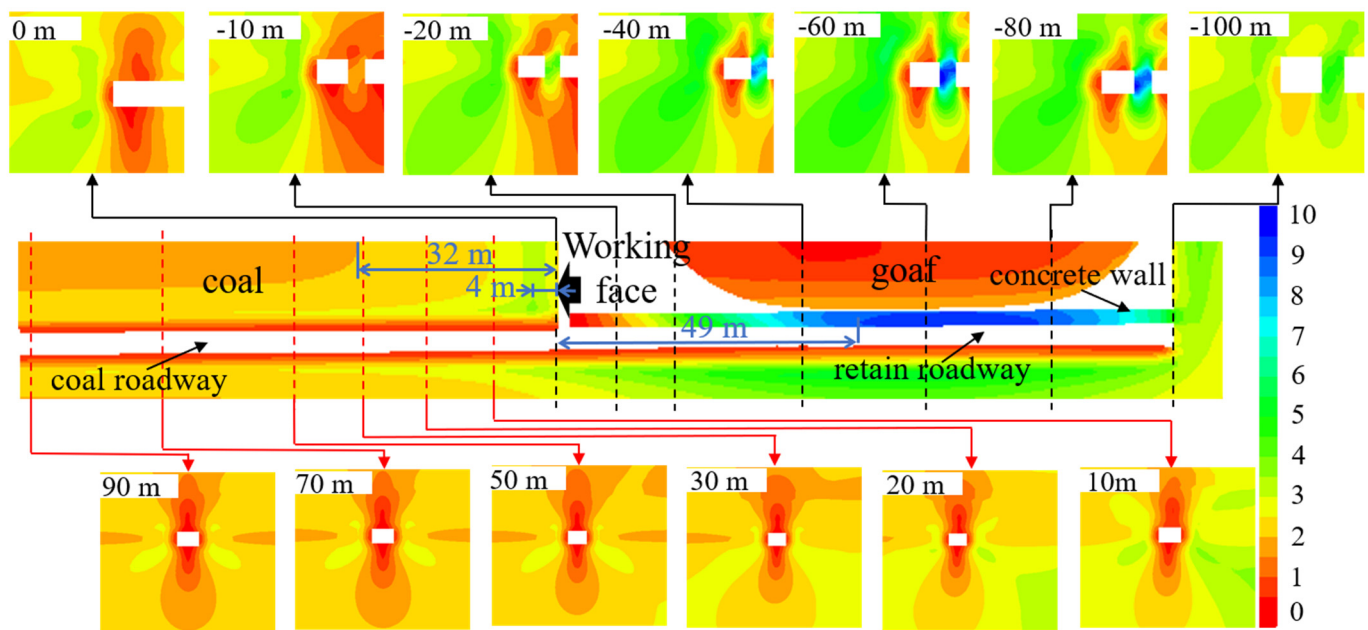


Figure 9. Distribution of deviatoric stress.

In Figure 9, the range of 0 m to -100 m is a mined-out area and the range of 0 m to 90 m is solid coal area. The influence range of advanced deviatoric stress is 32 m, and the distance between peak deviatoric stress and working face is 4 m. When the distance between the concrete wall and the working face is 49 m, the deviatoric stress in the concrete wall tends to be stable.

When the section position of roadway is 90 m, the peak deviatoric stress of roadway surrounding rock is mainly distributed in the roof and floor on both sides of the roadway, presenting a symmetrical butterfly shape distribution. When the section position of roadway is from 90 m to 30 m, the deviatoric stress of roof and floor is gradually connected. When the roadway section position is from 30 m to 0 m, the deviatoric stress has obvious deflection and concentration, the overall trend of the deviatoric stress of the roadway surrounding rock shifts to the entity coal side and the degree of deviatoric stress concentration of the roadway floor increases. When the section position of roadway is from 0 m to -10 m, the deviatoric stress peak position shifts from entity coal side to concrete wall side, and the deviatoric stress shape is an “oblique strip”. When the roadway section position is from -10 m to -80 m, the deviatoric stress peak value in the concrete wall increases and the shape of deviatoric stress is an “oblique 8 shape”. When the section position of roadway is from -80 m to -100 m, the deviatoric stress peak value decreases due to the coal wall support of the open-off cut and the shape of deviatoric stress is still an “oblique strip”.

In summary, when the roadway section position is from 90 m to -100 m, the deviatoric stress peak region shape of roadway surrounding rock is as follows: symmetrical butterfly shape, half-butterfly shape, narrow oblique strip shape, oblique 8 shape and wide oblique strip shape.

4.4.2. The Curve of Deviatoric Stress Distribution in Concrete Wall

Within the range of -2 ~ -100 m away from the working face, the deviatoric stress is monitored in different positions of the wall. The deviatoric stress monitoring points are arranged as shown in Figure 10 in which a, b, c and d represent the positions of concrete walls at various levels and the deviatoric stress distribution curve is shown in Figure 11.

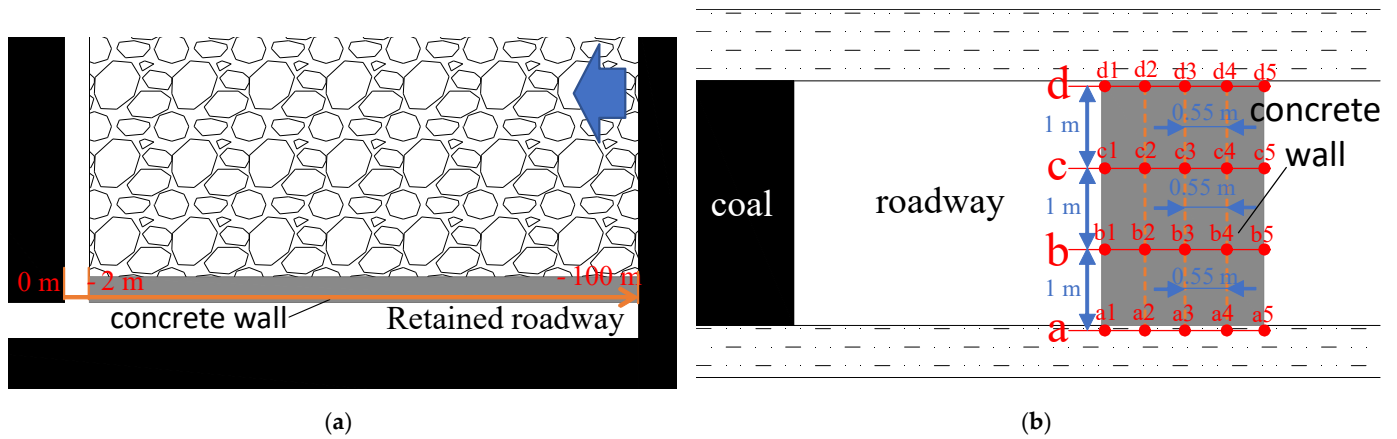


Figure 10. Layout of deviatoric stress monitoring points. (a) The plan of the roadway; (b) Cross-sectional view of roadway.

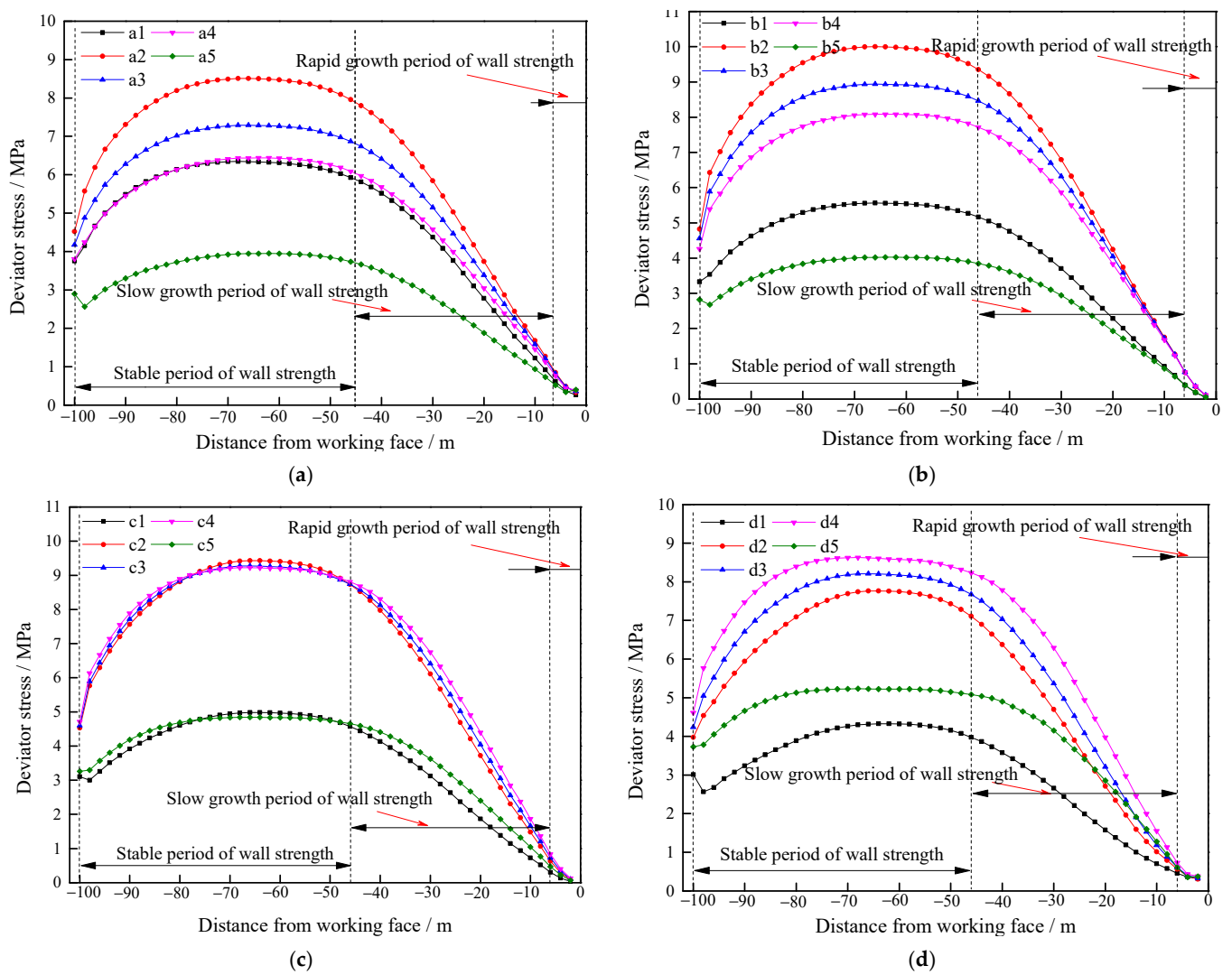


Figure 11. Distribution law of the deviatoric stress of concrete wall. (a) level of a; (b) level of b; (c) level of c; (d) level of d.

As shown in Figure 11, in the axial direction of the roadway, the deviatoric stress curves of each horizontal position are distributed in a “trapezoidal” shape. The strength growth period range of the concrete wall is $-2\sim-46$ m and the range of strength stability period is $-46\sim-100$ m. The peak position of deviatoric stress is mainly concentrated in $-46\sim-80$ m. The influence range of the solid coal side with open-off cut is about 20 m. With the increase of the distance between the concrete wall and the open-off cut of working face, the deviatoric stress in the concrete wall tends to rise until it reaches the peak value. The maximum strength position of the concrete wall is roughly the same as the position of the surrounding rock of the gob-side entry retaining into the stable state, indicating that the surrounding rock of the gob-side entry can enter into the stable state as soon as possible by shortening the time of the concrete wall reaching the maximum strength. At all levels of the concrete wall, the deviatoric stress values of the monitoring points from large to small are as follows: $a_2 > a_3 > a_4 > a_1 > a_5$, $b_2 > b_3 > b_4 > b_1 > b_5$, $b_2 > b_3 > b_4 > b_1 > b_5$ and $d_4 > d_3 > d_2 > d_5 > d_1$. In the vertical direction of the concrete wall, the deviatoric stress from large to small is $b_2 > c_2 > d_4 > a_2$ and the values of deviatoric stress are 9.99 MPa, 9.27 MPa, 8.63 MPa and 8.47 MPa, respectively. In the retained roadway, from the bottom to the top of the concrete wall, the peak deviatoric stress is transferred from the roadway side to the goaf side.

4.4.3. Deviatoric Stress Distribution of Surrounding Rock of Retained Roadway

At the section of -60 m from the working face, the deviatoric stress distribution of the surrounding rock is shown in Figure 12.

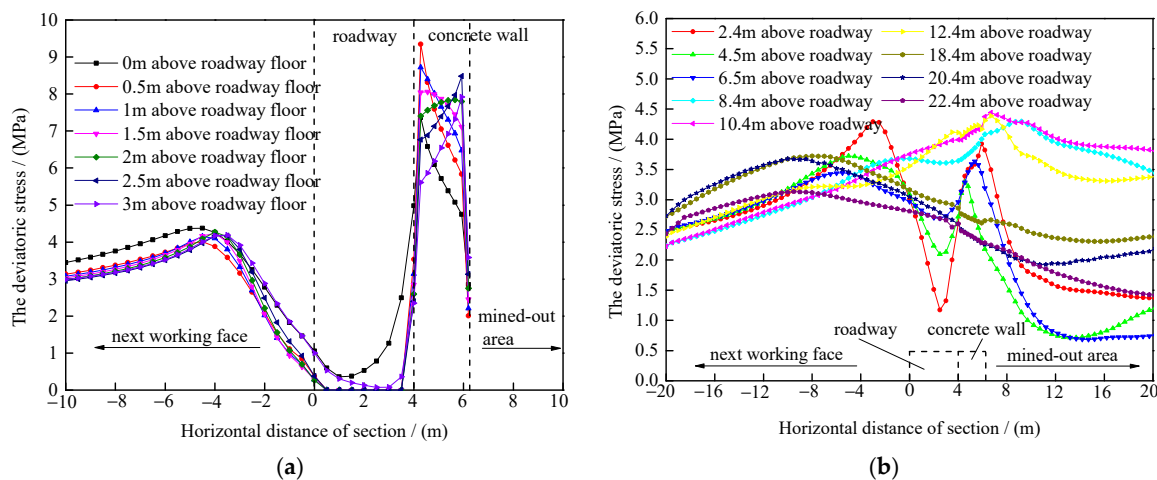


Figure 12. The deviatoric stress distribution of surrounding rock of the retained roadway. (a) Two sides of the retained roadway; (b) Roof of the retained roadway.

In Figure 12a, on the next working face side, with the increase of the distance from the roadway floor, the overall trend of the position of the peak deviatoric stress shifts to the roadway side, from 4.5 m to 3.5 m from the roadway edge. The change of the peak deviatoric stress is small, and the peak deviatoric stress is about 4.15 MPa. On the side of the concrete wall, with the increase of the distance from the roadway floor, the overall trend of the peak deviatoric stress position shifts to the goaf side, from 0.3 m to 1.9 m from the edge of the roadway, and the peak deviatoric stress is between 7.37 MPa and 8.48 MPa.

In Figure 12b, on the side of the next working face, with the increase of the distance from the roadway roof, the overall trend of the peak deviatoric stress position is a fluctuating trend, that is, the peak deviatoric stress position fluctuates between deviating to the roadway edge and away from the roadway edge, and the peak deviatoric stress is between 3.13~4.38 MPa. Similarly, on the side of the concrete wall, with the increase of the distance from the roadway roof, the overall trend of the deviatoric eccentric stress position is a fluctuating trend, and the peak deviatoric stress is between 3.23~4.43 MPa.

The deviatoric stress tensor causes the rupture of rock mass element, and the change of the peak deviatoric stress position in roadway surrounding rock is complex. The peak deviatoric stress position in the roadway surrounding rock is plotted, as shown in Figure 13.

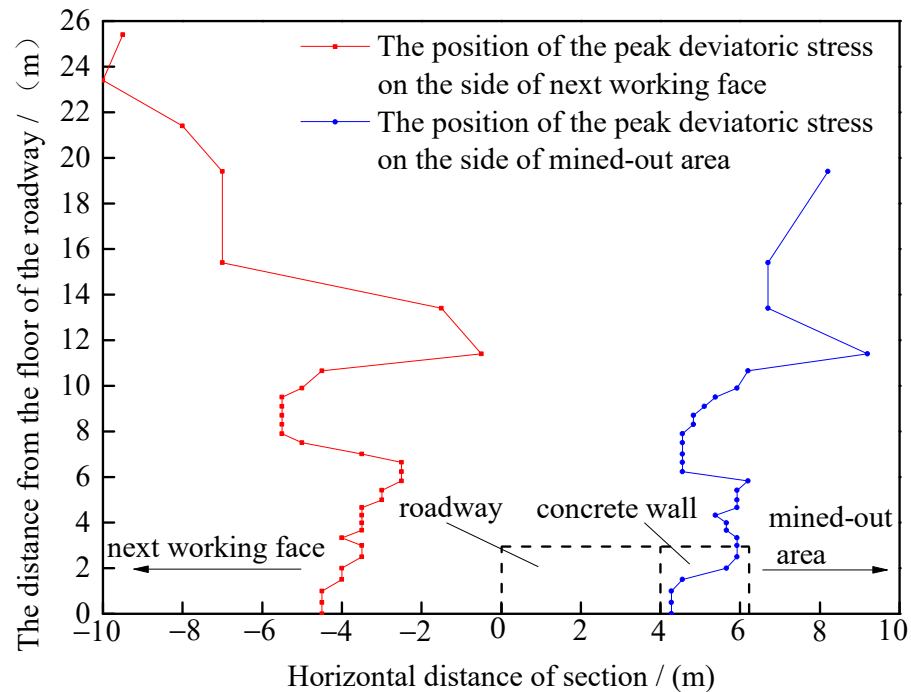


Figure 13. Diagram of the peak deviatoric stress position.

As can be seen from Figure 13, in the vertical direction, within the range of 0 m to 6 m from the retained roadway floor, the position of the peak deviatoric stress on both sides of the roadway is offset to the side of the mined-out area. Within the range of 6 m to 19.4 m from the retained roadway floor, the position of the peak deviatoric stress on both sides of the roadway roof is the trend of left and right fluctuation. In the range of 19.4 m and above from the reserved roadway floor, the peak deviatoric stress is distributed on the next working face side and the distribution form of deviatoric stress changes from double peak distribution to single peak distribution.

4.5. Damage of Surrounding Rock of Roadway

In the range of 90 m in front of the working face to 100 m in the lagging working face, damage of the surrounding rock of roadway is shown in Figure 14.

In Figure 14, when the position of the roadway section is 90 m, the main failure mode of the two sides of the roadway is shear failure, the damage depth on both sides of the roadway is 3 m, the main failure mode of the roof and floor of the roadway is compression failure, the damage depth of the roof and floor of the roadway are 0.3 m and 1 m, respectively. With the cross section of the roadway being closer to the working face, the damage area of the solid coal side of the roadway and the damage area of the roadway roof extend to the solid coal side, while the damage area of the roadway floor extends to the side of the working face, which is approximately consistent with the variation characteristics of the deviatoric stress in Figure 9.

In the area of the lagging working face, that is, the position of the roadway section from 0 m to -100 m, with the increase in the distance of the lagging working face, the damaged area of the surrounding rock of the retained roadway is significantly increased. The damaged area of the roof of the retained roadway gradually runs through. The damaged area of the floor of the retained roadway extends to the bottom of the concrete wall. In the retained roadway, the damaged area on the solid coal side extends to the deep and the maximum depth of damaged area is 6 m. Concrete wall is in the state of

shear damage and compression damage. This is because the strength of the concrete wall is very small at the early stage of pouring and the movement of the roof and floor leads to the deformation of the concrete wall. However, over an increasing length of time, the strength of the concrete wall continues to increase, and the state of the concrete wall can still maintain integrity and stability.

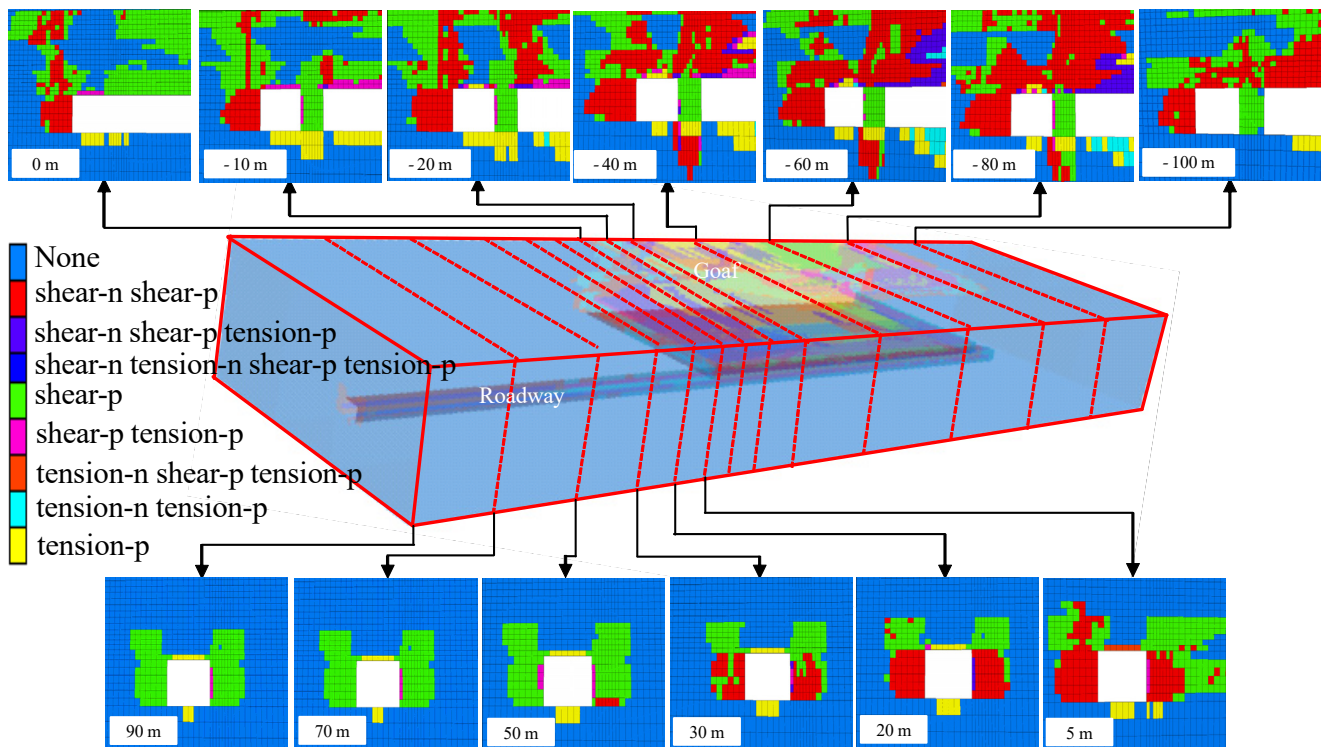


Figure 14. Damage to the surrounding rock of the roadway.

Based on the above analysis of the distribution law of the deviatoric stress and the damaged area of the surrounding rock, it can be seen that the deviatoric stress and the damaged area of the surrounding rock of the retained roadway show obvious asymmetric distribution characteristics. In the retained roadway, the deviatoric stress of the concrete wall side is obviously larger than that of the solid coal side, and the damaged area of the middle and lower part of the solid coal side is larger than that of the upper part of the solid coal side. Because the damage range of the roof and solid coal pillar side of the retained roadway is larger than range controlled by ordinary bolt support, in order to ensure the stability of the retained roadway, it is necessary to use anchor cable to control the surrounding rock on the roof and solid coal side of the retained roadway. In the retained roadway, the concrete wall is always affected by the movement trend of the roof and floor. After the concrete wall is poured, the compressive strength of the concrete wall needs 4 days to increase to 11.64 MPa. Therefore, the strengthening support technology is adopted for the concrete wall during this period of time to avoid the overall instability of the concrete wall caused by insufficient strength or excessive deformation.

5. The Control Mechanism and Technology of Roadway Surrounding Rock

5.1. The Supporting Mechanism of the Surrounding Rock

In the roadway retained behind the working face, shear failure of the surrounding rock occurs under the action of deviatoric stress, which reduces the stability of the surrounding rock. Based on the distribution characteristics of deviatoric stress and damage zone, the outline line of deviatoric stress peak value and damage zone are drawn, as shown in Figure 15.

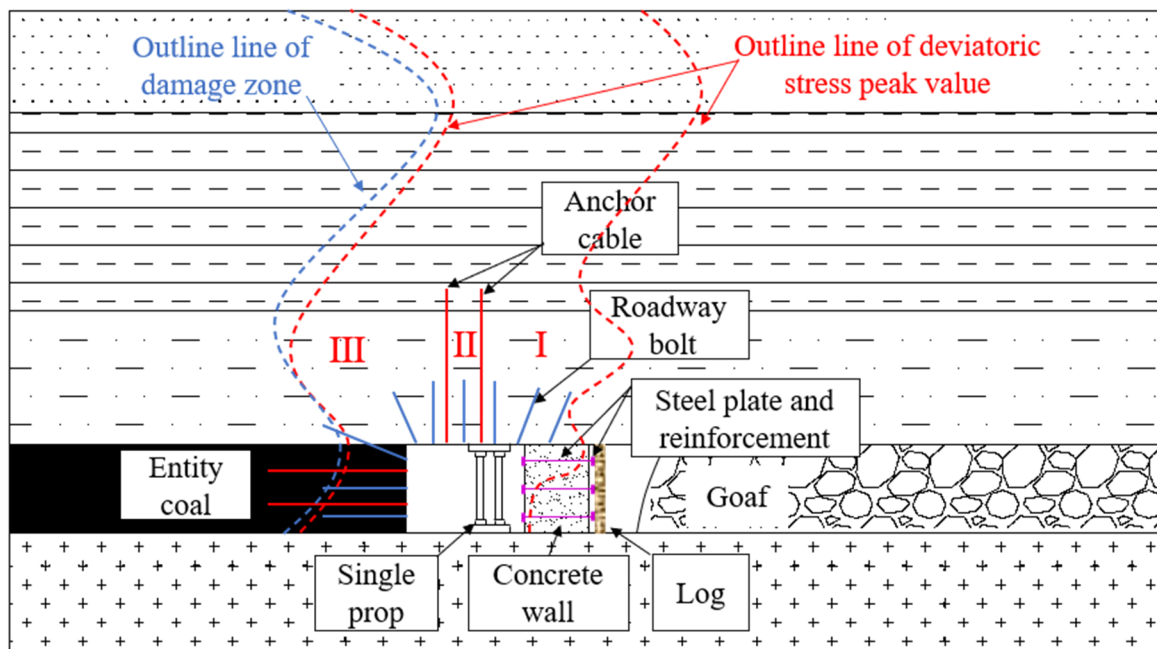


Figure 15. The outline line of deviatoric stress peak value and plastic zone.

It can be seen from Figure 15 that the outline line of deviatoric stress peak value on the entity coal side is very close to the outline line of damage zone, indicating that deviatoric stress is the essence of rock mass failure. Based on the distribution of the deviatoric stress outline line in the surrounding rock of the retained roadway, the zoning control technology of the retained roadway surrounding rock is put forward: (1) Bolt support is added to the roof of concrete wall. (2) The concrete wall is reinforced with tensile steel bars and steel plates. (3) Double rows of single pillars are arranged in the retained roadway to protect the concrete wall. (4) Round logs are arranged in the goaf to stabilize the filling model. (5) High-strength pretightening anchor cable support should be added at the entity coal side and roof of the retained roadway. The surrounding rock of retained roadway can be divided into three areas, namely, the area of concrete wall side (I), the area of roadway roof (II) and the area of entity coal side (III). The surrounding rock control mechanism is described below.

- (1) Research shows [24] that it is necessary to control the stability of the rock mass in the area surrounded by outline line of peak deviatoric stress. The anchor cable passes through the outline line of deviatoric stress peak value, which can control the unstable rock mass between the outline line of the deviatoric stress peak value and the roadway edge. Therefore, in zone III, the anchor cable passing through the outline line of the deviatoric stress peak and the outline line of the damage zone can combine the shallow bearing structure with the deep bearing structure to form a composite bearing structure. The formation of the composite structure can effectively change the stress state of the surrounding rock, restrain the deformation and tension-shear failure of the surrounding rock and, finally, maintain the integrity of the surrounding rock [10].
- (2) In zone I, the anchor rod is added to the roof strata to enhance the integrity of the overlying rock of the filling area. The compressive strength of the concrete wall reaches 10.87 MPa after being filled for 3 days, so the single hydraulic support is arranged in the gob-side entry as temporary reinforcement support. Before the strength of the concrete wall reaches the required strength, the single hydraulic support can provide larger support resistance, bear the roof load, control the separation of the roof strata, control the rotation rate of the roof, but also can transfer the pressure of the overburden to the floor, and exert reverse binding force on the floor and play a role

in controlling floor-heave. Reinforcement with steel bars and iron plates should be adopted for the wall, because the concrete wall can form a strong bearing structure under the reinforcement of steel bars and plates, which not only inherits the stiffness of concrete but, also, under the three-dimensional compression under the action of a lateral binding force, and its own bearing capacity, structural integrity and stability are significantly improved, and greatly limit the lateral deformation of concrete and prevent its excessive large deformation [25,26].

- (3) In zone II, the form of combined support of anchor cable and anchor rod is implemented. Combined support can connect the shallow bearing structure with the deep bearing structure to form a composite bearing structure and inhibit the separation of roof strata [27].

5.2. Parameters of Support

On the entity coal side of the roadway, the spacing and row spacing of screwing threaded steel bolts are 900 mm and 900 mm, and the spacing and row spacing of anchor cables of high strength and high pretension are 950 mm and 900 mm. At the roof of the roadway, the spacing and row spacing of screwing threaded steel bolts are 900 mm and 900 mm, and the spacing and row spacing of anchor cables of high strength and high pretension are 1600 mm and 900 mm. On the side of the concrete wall of the roadway, the spacing and row spacing of the reinforcing steel bar are 750 mm and 900 mm, and the thickness \times length \times width of the steel plate is 10 mm \times 200 mm \times 200 mm. The log is close to the concrete wall, and the distance between the logs is 1000 mm. The cushioning wood is added on the top of the single pillars, and the spacing and row spacing of the single pillars are 1200 mm and 1500 mm. The roof of the concrete wall and the roof of the retained roadway are arranged with a metal mesh of a 50 mm \times 50 mm diamond mesh and a steel bar ladder made of $\phi 12$ mm steel for joint support, and the roadway support is shown in Figure 16.

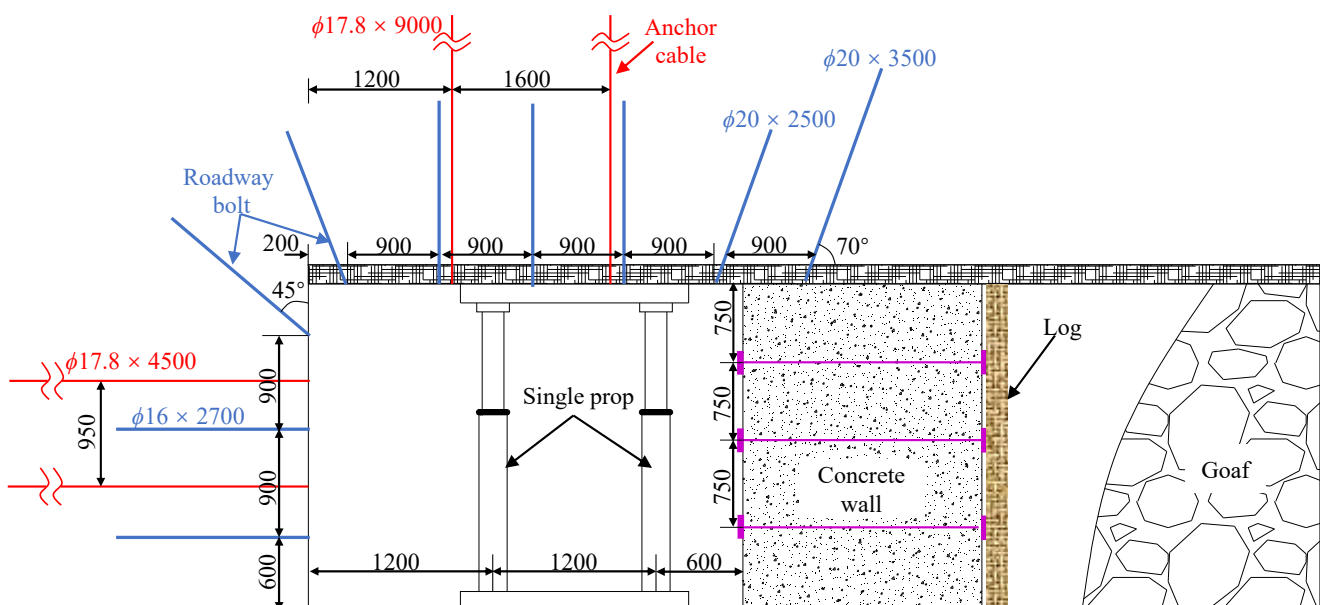


Figure 16. Schematic diagram of the retained roadway support.

5.3. Deformation of Retained Roadway

In order to verify the rationality of supporting parameters, the deformation of roof, floor, entity coal side and concrete wall side of roadway is continuously monitored. The continuous monitoring time is 30 days, and the monitoring position is 60 m away from the open cut of the working face. The deformation amount and deformation rate of the retained roadway are shown in Figure 17.

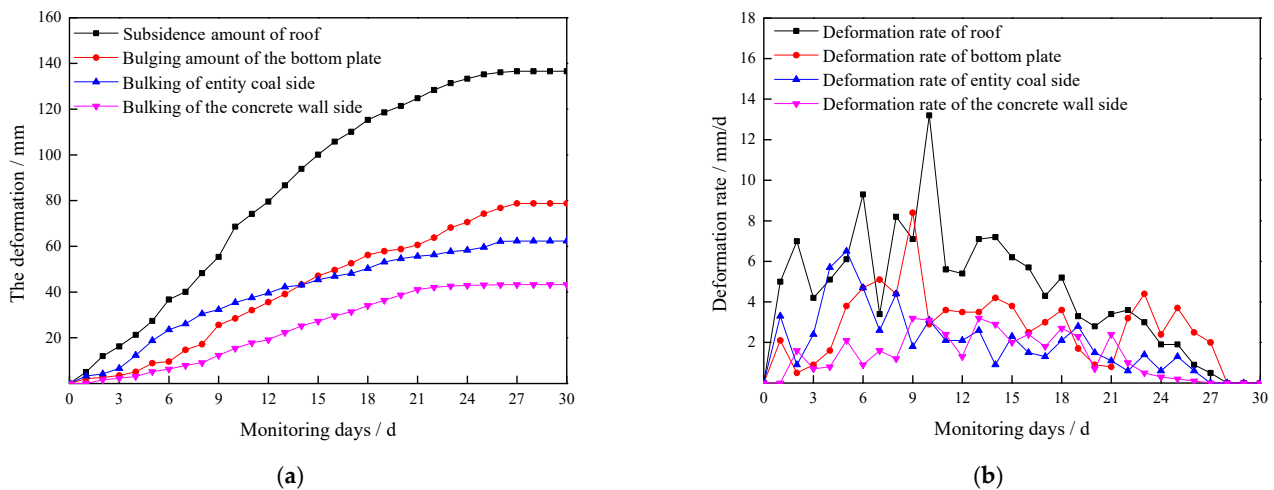


Figure 17. Deformation amount and deformation rate of the retained roadway (a) Deformation of roadway surrounding rock; (b) Deformation rate of roadway surrounding rock.

Through continuous monitoring, it is known that the deformation rate of the surrounding rock of the retained roadway is larger from the 1st day to the 15th day of retained roadway, and the average deformation rates of roof, floor, entity coal side and concrete wall side are 6.67 mm/d, 3.53 mm/d, 3.03 mm/d and 1.93 mm/d. The maximum deformation rates of the roof, floor, entity coal side and concrete wall side are 13.2 mm/d, 8.4 mm/d, 6.5 mm/d and 3.2 mm/d, respectively. After the 15th day on the retained roadway, the deformation rate of the surrounding rock decreases. After 25 days, the surrounding rock of retained roadway remains stable, in which the maximum deformation of roof, floor, entity coal side and concrete wall side is 136.6 mm, 78.8 mm, 62.3 mm and 43.3 m, respectively.

The surrounding rock deformation of the retained roadway is measured within the range of 60 m behind the working face. The retained roadway deformation in the range of 60 m behind the working face is shown in Figure 18.

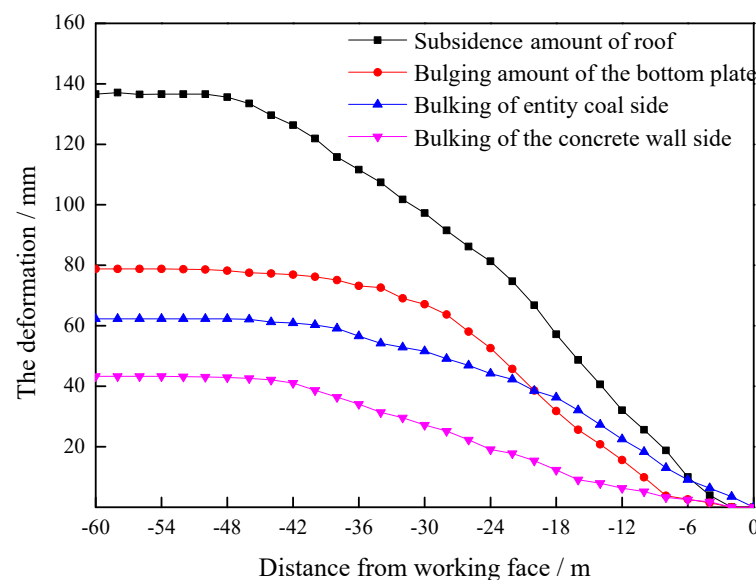


Figure 18. Deformation of surrounding rock of retained roadway.

As can be seen from Figure 18, the roof, floor, entity coal side and concrete wall side of the retained roadway are stable at 46 m, 40 m, 46 m and 48 m from the working face, respectively. There is no bending and fracturing phenomenon in the single pillar and

concrete wall in the retained roadway, which shows that the supporting scheme of the retained roadway can meet the stability of the surrounding rock.

6. Conclusions

- (1) The periodic pressure frequency of the working face is 3 to 4 days. In order to retain the roadway, the strength of the filled wall in the roadway should be at least between 10.16 MPa and 11.64 MPa. When the width of the concrete wall is 2.2 m, the strength of the concrete wall can reach 10.87 MPa~11.64 MPa in 3 to 4 days, so the width of the concrete wall in the retained roadway is 2.2 m.
- (2) The influence range of deviatoric stress in front of the working face is 32 m, and the distance between peak deviatoric stress and the working face is 4 m. When the distance of the lagging working face is 49 m, the retained roadway tends to be stable.
- (3) From the position of 90 m in front of the working face to the position of 100 m behind the working face, the distribution form of the roadway surrounding rock deviatoric stress is: symmetrical butterfly shape → single butterfly shape → narrow oblique strip → oblique 8 shape → wide oblique strip shape.
- (4) Based on the distribution characteristics of the deviatoric stress and damage zone in the surrounding rock of retained roadway, the surrounding rock of retained roadway is divided into three regions with the boundary of the peak deviatoric stress outline line and the damage zone outline line, and different supporting forms are adopted in three regions.
- (5) After field application and measurement, the surrounding rock deformation of the retained roadway is effectively controlled, and the maximum deformation of roof, floor, solid coal side and concrete wall side is 136.6 mm, 78.8 mm, 62.3 mm and 43.3 mm, respectively.

Author Contributions: Z.W. and J.Z. contributed to the formulation of the overarching research goals and aims; J.L. and P.W. helped to review this paper; C.W. and L.S. amended this paper. All authors have read and agreed to the published version of the manuscript.

Funding: This research is supported by the National Natural Science Foundation of Surface Project of China (No. 51774289), the National Natural Science Foundation of the Youth Science Foundation of China (No. 51404270) the Open Fund of State Key Laboratory of Green and Safe Development of Western Coal (SKLCRKF1903), the National Natural Science Foundation of Surface Project of China (No. 52074291).

Informed Consent Statement: Informed consent was obtained from all subjects involved in the study.

Conflicts of Interest: The authors declare no conflict of interest.

References

1. Yang, Y.; Bai, J.B.; Wang, X.Y.; Zhang, L.Y. Control of the Surrounding Rock of a Goaf-Side Entry Driving Heading Mining Face. *Sustainability* **2020**, *12*, 2623.
2. Yang, H.Q.; Han, C.L.; Zhang, N. Stability Control of a Goaf-Side Roadway under the Mining Disturbance of an Adjacent Coal Working Face in an Underground Mine. *Sustainability* **2019**, *11*, 6398. [[CrossRef](#)]
3. Thorntin, C.; Zhang, L. On the evolution of stress and micro-structure during general 3D deviatoric straining of granular media. *Geotechnique* **2010**, *60*, 333–341. [[CrossRef](#)]
4. Tian, M.L.; Han, L.J.; Meng, Q.B. Physical Model Experiment of Surrounding Rock Failure Mechanism for the Roadway under Deviatoric Pressure from Mining Disturbance. *KSCE J. Civ. Eng.* **2020**, *24*, 1103–1115. [[CrossRef](#)]
5. Xue, D.J.; Yang, J.X.; Wu, F.F. Analysis of fracture mechanism for surrounding rock hole based on water-filled blasting. *Int. J. Coal Sci. Technol.* **2020**, *7*, 704–713.
6. Zhang, C.; Zhao, Y.X.; Bai, Q.S. 3D DEM method for compaction and breakage characteristics simulation of broken rock mass in goaf. *Acta Geotech.* **2021**. [[CrossRef](#)]
7. Tan, Y.L.; Fan, D.Y.; Liu, X.S. Numerical investigation of failure evolution for the surrounding rock of a super-large section chamber group in a deep coal mine. *Energy Sci. Eng.* **2019**, *7*, 3124–3146. [[CrossRef](#)]
8. Tan, Y.L.; Ma, Q.; Zhao, Z.H. Cooperative bearing behaviors of roadside support and surrounding rocks along gob-side. *Geomech. Eng.* **2019**, *18*, 439–448.

9. Ma, Q.; Tan, Y.L.; Zhao, Z.H. Roadside support schemes numerical simulation and field monitoring of gob-side entry retaining in soft floor and hard roof. *Arab. J. Geosci.* **2018**, *11*, 563–569. [[CrossRef](#)]
10. Du, Z.W.; Chen, S.J.; Ma, J.B. Gob-Side Entry Retaining Involving Bag Filling Material for Support Wall Construction. *Sustainability* **2020**, *12*, 6353. [[CrossRef](#)]
11. Tian, Z.J.; Zhang, Z.Z.; Deng, M. Gob-Side Entry Retained with Soft Roof, Floor, and Seam in Thin Coal Seams: A Case Study. *Sustainability* **2020**, *12*, 1197. [[CrossRef](#)]
12. Luan, H.J.; Jiang, Y.J.; Lin, H.L. Development of a New Gob-Side Entry-Retaining Approach and Its Application. *Sustainability* **2018**, *10*, 470. [[CrossRef](#)]
13. Zhang, N.; Han, C.L.; Kan, J.G. Theory and practice of surrounding rock control for pillarless gob-side entry retaining. *J. China Coal Soc.* **2014**, *39*, 1635–1641.
14. Xie, E.B. Influence factors on stability of surrounding rocks of gob-side entry retaining in top-coal caving mining face. *Chin. J. Rock Mech. Eng.* **2004**, *23*, 3059–3065.
15. Yu, W.J.; Wu, G.S.; Yuan, C. Failure characteristic sand engineering stability control of roadway. *J. China Coal Soc.* **2017**, *42*, 1408–1419.
16. Wang, J.F.; Wang, E.; Chen, D.D. Evolution of deviatoric stress and control of surrounding rock at gob-side entry retaining with narrow flexible-formwork wall. *J. China Coal Soc.* **2021**, *46*, 1220–1231.
17. Ma, N.J.; Li, J.; Zhao, Z.P. Distribution of the deviatoric stress field and plastic zone in circular roadway surrounding rock. *J. China Univ. Min. Technol.* **2015**, *44*, 206–213.
18. Xu, L.; Wei, H.X.; Xiao, Z.Y. Engineering cases and characteristics of deviatoric stress under coal pillar in regional floor. *Chin. J. Geotech. Eng.* **2015**, *36*, 561–568.
19. Li, J.Z.; Zhang, M.; Li, Y.; Hu, H. Surrounding rock control mechanism in the gob-side retaining entry in thin coal seams, and its application. *J. S. Afr. Inst. Min. Metall.* **2018**, *118*, 471–480. [[CrossRef](#)]
20. Kan, J.G.; Zhang, N.; Li, B.Y. Analysis of supporting resistance of backfilling wall for gob-side entry retaining under typical roof conditions. *Rock Soil Mech.* **2011**, *32*, 2778–2784.
21. Ning, J.G.; Ma, P.F.; Liu, X.S. Supporting mechanism of “yielding-supporting” beside roadway maintained along the goaf under hard rocks. *J. Min. Saf. Eng.* **2013**, *30*, 369–374.
22. Ma, L.Q.; Zhang, D.S.; Chen, T. Study on packing body supporting resistance of enter-in packing for in-situ gob-side entry retaining in fully-mechanized top-coal caving mining face. *Chin. J. Rock Mech. Eng.* **2007**, *26*, 544–550.
23. Hua, X.Z. Study on gob-side entry retaining technique with road-side packing in longwall top-coal caving technology. *J. Coal Sci. Eng. (China)* **2004**, *10*, 9–12.
24. Xie, S.R.; Yue, S.S.; Chen, D.D. Deviatoric stress evolution laws and control of surrounding rock at gob-side entry retaining in deep backfilling mining. *J. China Coal Soc.* **2018**, *43*, 1837–1846.
25. Girgin, Z.C.; Arioglu, N.; Arioglu, E. Evaluation of strength criteria for very-high-strength concretes under triaxial compression. *ACI Struct. J.* **2007**, *104*, 278–284.
26. Deng, Z.H.; Wang, Y.M.; Sheng, J. Strength and deformation of recycled aggregate concrete under triaxial compression. *Constr. Build. Mater.* **2017**, *156*, 1043–1052. [[CrossRef](#)]
27. Feng, G.R.; Wang, P.F.; Chugh, Y.P. Stability of gate roads next to an irregular yield pillar: A case study. *Rock Mech. Rock Eng.* **2019**, *52*, 2741–2760. [[CrossRef](#)]